Research Article Vol. 30, No. 3 / 31 Jan 2022 / Optics Express 4084
Optics EXPRESS

Dual-band polarization-insensitive toroidal dipole quasi-bound states in the continuum in a permittivity-asymmetric all-dielectric meta-surface

SHILIN YU,[1,2] YUSEN WANG,[1,2] ZIANG GAO,[1,2] HAO LI,[1,2] SHAOZHE SONG,[1,2] JIANGUO YU,[1,2] AND TONGGANG ZHAO[1,2,*]

[1]*Beijing Key Labroratory of Space-Ground Interconnecton and Convergence, Beijing University of Posts and Telecommunications, Beijing 100876, China*
[2]*School of the Electronic and Engineering, Beijing University of Posts and Telecommunications, Beijing 100876, China*
[*]*zhaotg@bupt.edu.cn*

Abstract: Ultra-high quality (Q) factor resonances derived from the bound states in the continuum (BICs) have drawn much attention in optics and photonics. Especially in meta-surfaces, they can enable ultrasensitive sensors, spectral filtering, and lasers because of their enhanced light-matter interactions and rare superiority of scalability. In this paper, we propose a permittivity-asymmetric all-dielectric meta-surface, comprising high-index cuboid tetramer clusters with symmetric structural parameters and configuring periodically on a glass substrate. Simulation results offer dual-band quasi-BICs with high Q values of 4447 and 11391, respectively. Multipolar decomposition in cartesian and electromagnetic distributions are engaged to analyze the physical mechanism of dual quasi-BIC modes, which reveals that they are both governed by magnetic quadrupole (MQ) and in-plane toroidal dipole (TD). The polarization-insensitive and scalable characteristics are also investigated. Additionally, we appraise the sensing performances of the proposed structure. As an example, our work supports an uncommon route to design dual-band polarization-insensitive TD quasi-BICs resonators and facilitates their applications in optic and photonics, such as low-threshold lasers and sensing.

1. Introduction

Ultra-narrow resonances, meaning ultra-high quality (Q) factor and ultra-low losses in meta-surfaces, can find extensive applications in optics and photonics including but not limited to narrowband absorbers [1,2], slow-light devices [3], highly sensitive sensing [4,5], and filters [6]. Utilizing appropriate material choice and optimal meta-surface design can lower the non-radiative or radiative losses to obtain ultra-high Q resonance states. Traditionally, metallic meta-surfaces act a pivotal part in nanophotonic devices [7–9], while high inherent losses of metals [10] block them to excite resonances with ultra-high Q factor. Therefore, all-dielectric meta-surfaces, especially high-index all-dielectric meta-surfaces (HIADMS), such as silicon/germanium-based meta-atom or meta-molecule structures, have been investigated and employed. They can support Mie resonances with extremely low losses, enhance light-matter interactions by the strong confinement of electromagnetic field, and be compatible with complementary metal-oxide-semiconductor (CMOS) technology, which makes them be a promising alternative to metal or hybrid metamaterials in optic and photonic systems [11–14].

Bound state in the continuum (BIC) manifests a wave that acts as a localized state in dynamic systems [15] whilst coexisting with a continuous spectrum of radiating waves. They are generally divided into two patterns, symmetry-protected BIC [16] and accidental BIC [17,18]. Accidental BIC reveals the coincidental vanishment of the coupling constants with all radiating waves

#448933 https://doi.org/10.1364/OE.448933
Journal © 2022 Received 17 Nov 2021; revised 17 Jan 2022; accepted 17 Jan 2022; published 24 Jan 2022

Optics EXPRESS

by adjusting structural parameters continually [19,20]. In contrast, symmetry-protected BIC explains the destructive interference when the vanishment of the coupling constants derives from structural symmetry [21–23]. Authentically optical BICs, however, survive just as a mathematical concept with zero linewidth and infinite Q-factor in unattainable lossless infinite structures [12,22]. To be employed in real optical systems, a so-called quasi-BIC is transformed from BIC, which manifests finite but extremely high Q value and ultra-narrow resonant linewidth [24] because of the tiny channel of coupling to free space radiation from structural asymmetry. One can carry out the accurate control of radiation losses from quasi-BIC in periodic structures by manipulating the introduced asymmetry in the unit cell [22] to achieve the on-demand high-Q states. Consequently, quasi-BICs from symmetry-protected BICs have attracted much more attention and been demonstrated in HIADMS [25].

Among all the configurations for quasi-BICs in HIADMS, structural asymmetry in the cluster has been widely reported [22,25–27]. However, most current studies concentrate on the geometric asymmetry in meta-atom, such as the area asymmetry [26–28]. Additionally, the relative geometric relation of each unit cell can be asymmetric whilst they are symmetric in themselves, such as in [25,29,30]. As a consequence, the meta-molecule of the meta-surface will perform asymmetry or even chirality as an entirety. Another method is to tailor the physical properties of every meta-atom for symmetric breaking (such as the permittivity or refractive index [12]) in meta-surfaces. Nevertheless, investigations for permittivity asymmetry in HIADMS are still not enough, which expect further exploration in structure design and physical analysis.

Polarization sensitive [12,23,25–28] is highly common in the excited resonances driven by symmetry-protected BIC because the in-plane or out-of-plane asymmetry introduced is always along a certain direction to damage the rotational symmetry or mirror symmetry of the structures. To excite polarization-independent quasi-BIC in HIADMS, some meta-surface configurations have been proposed, such as cuboid multimer [30], asymmetric circular hollows array [31], multi-disks supercell [32,33], and nano-cylinder [34]. Overall, most of them are demonstrated based on geometric structural asymmetry. Rare proof of polarization-independent quasi-BIC excited based on permittivity asymmetry in HIADMS is discussed, which is definitely worthwhile to do further exploration.

Recently, some works have been demonstrated, such as symmetry analysis of trimer-based all-dielectric metasurfaces with toroidal dipole modes [35], theoretical analysis of TDBIC [36], quasi-BIC in silicon metasurface for refractometric sensing, and tunable notch filtering [37], and ultra-high Q factor resonant dielectric metasurfaces based on hollow nanocuboids [38]. Nevertheless, research on dual-band polarization-insensitive TD quasi-BIC based on permittivity-asymmetric all-dielectric meta-surface is extremely rare but significant to provide an uncommon route. In this letter, we propose a permittivity-asymmetric all-dielectric meta-surface, which supports dual-band polarization-insensitive TD quasi-BIC modes. The meta-surface comprises high-index cuboid tetramer clusters with symmetric structural parameters and configures periodically on a glass substrate. We first demonstrate the BIC characteristics of dual-band resonances and choose the combination of Si and InAs as the permittivity-asymmetric materials. The dual-band quasi-BICs show ultra-high Q values of 4447 and 11391, respectively. And then, multipolar decomposition in cartesian and electromagnetic distributions are engaged to analyze the physical mechanism of dual quasi-BIC modes, which reveals that they are both governed by MQ and in-plane toroidal dipole (TD). We next investigate the polarization-insensitive and scalable characteristics of the permittivity-asymmetric meta-surface. Finally, the sensing performance of the proposed structure is appraised and theoretically analyzed by perturbation theory. As an instance, our work supports an uncommon route to design dual-band polarization-insensitive TD quasi-BICs resonators and facilitates their applications in optic and photonics, such as low-threshold lasers and sensing.

Optics EXPRESS

2. Structure design

Figure 1 offers structural parameters and details of the designed meta-surface. The meta-molecule is a high-index tetramer cluster, which is constituted of four same cuboids named as a_1, a_2, a_3, and a_4, respectively. Herein, we introduce a scaling factor S. Each cuboid has a square surface with a length of $S\times L$ and the height of $h = 200$ nm throughout the paper. The surface of the unit cell is also square with a length of $S\times P$. And we fix the intra-cluster distance between the centers of cuboids as $(S\times P)/2$ in both the x and y-axis. When the scalable factor $S = 1$, the parameters L and P are given as 340 nm and 800 nm, respectively. The substrate of the proposed structure is glass with a height of 600 nm, whose data are from the Palik handbook [39] and dispersion curve is shown in Fig. 3(d). Herein, we divide the meta-atoms into two groups. The first group (FG) consists of a_1 and a_4. Simultaneously, a_2 and a_3 are named as the second group (SG). To excite dual-band polarization-insensitive TD quasi-BICs, FG and SG are given different refractive index materials. We performed the numerical calculation by FDTD Solutions based on the finite-difference time-domain (FDTD) method. And periodic boundary conditions are employed in both x and y directions. Additionally, we set the perfectly matched layers (PMLs) above

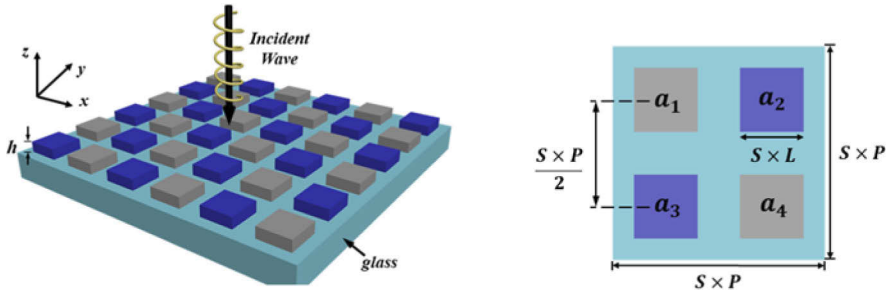

Fig. 1. Schematic diagram of the designed permittivity-asymmetric meta-surface including periodically high-index tetramer cluster. The meta-molecule is constituted of four same cuboids with the length of $S\times L$ and thickness of $h = 200$ nm. $(S\times P)/2$ is the intra-cluster distance between the centers of cuboids. The surface of the unit cell is also square with a length of $S\times P$.

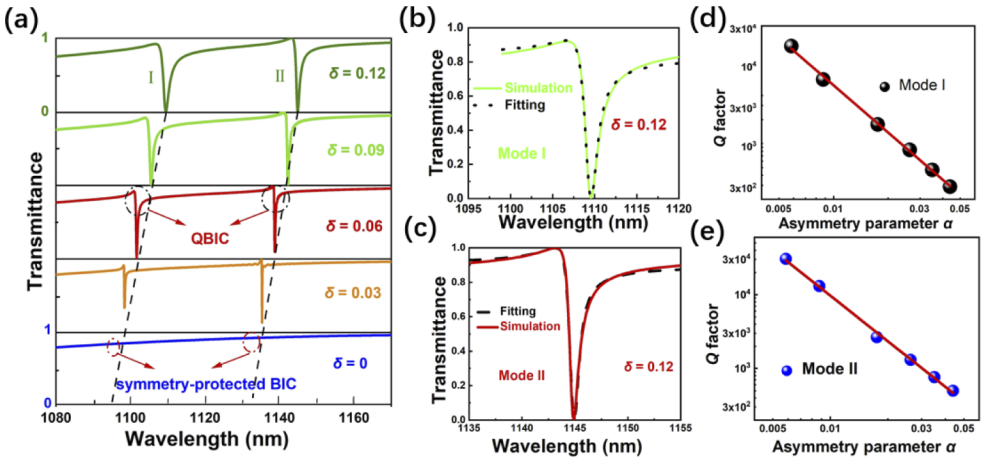

Fig. 2. (a) Transmission spectra of the permittivity-asymmetric meta-surface with varying refractive index differences. Fano fitting of (b) mode I and (c) mode II when δ=0.12. The Q factor as a function of α at the logarithmic axis of (d) mode I and (e) mode II.

Optics EXPRESS

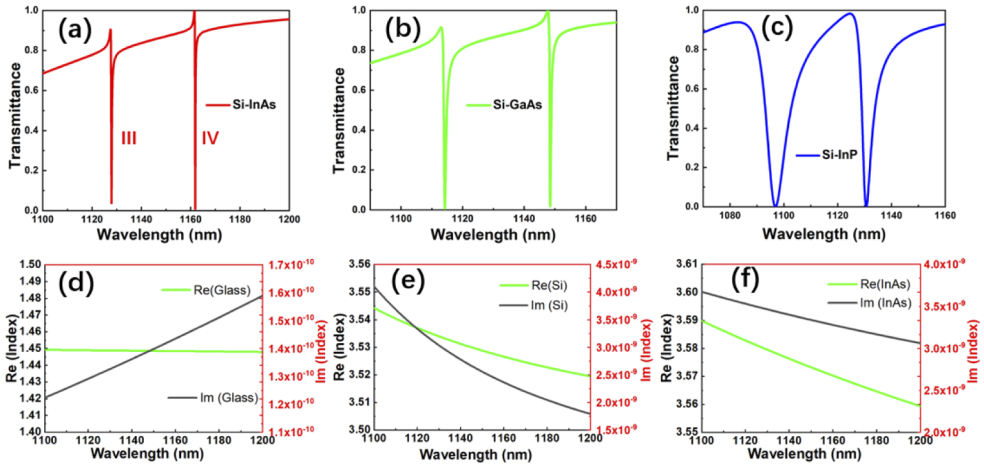

Fig. 3. Transmission spectra with different material combinations in the proposed meta-surface: (a) Si-InAs, (b) Si-GaAs, (c) Si-InP. The dispersion curves of materials (d) glass, (e) Si, and (f) InAs.

and under the meta-molecule. The plane wave electric field is polarized along the x-direction (polarization angle $\theta = 0$) and the wave vector is along the z-direction, as shown in Fig. 1.

3. Results and discussions

3.1. Permittivity asymmetry to excite dual quasi-BICs in meta-surface

The mechanism of the transformation from symmetry-protected BIC to quasi-BIC is that new radiation channels are built for incident light radiating to free space when the symmetry of the meta-surface is broken. To demonstrate the excitation of quasi-BIC, we first set the FG as an unchanged refractive index n_1 of 3.42 and the SG as a refractive index parameter n_2. Consequently, the asymmetry parameter can be detailed as $\alpha = \delta/n_1$, where $\delta = n_2 - n_1$ means the refractive index difference between FG and SG. The calculated transmission spectra of changing δ from 0 to 0.12 are displayed in Fig. 2(a), where two Fano-like resonances emerge when $\delta \neq 0$, named as mode I and II, respectively. One can be observed that the resonant modes are sharper and sharper as the δ decreases gradually. Until $\delta = 0$, modes I and II have disappeared, which means that the radiation channels are closed and no energy can be leaked to the free space continuum. Therefore, the two Fano resonances can be recognized as quasi-BIC modes and the permittivity asymmetry leads to the transformation from symmetry-protected BIC. Meanwhile, nearly linear redshifts of the resonant wavelengths for the two modes occur in the two modes (marked by the dotted line in Fig. 2(a)). That's because the effective refractive index of the meta-surface increases with the growth of δ.

Even though they are not infinitely high Q factor as symmetry-protected BICs perform, quasi-BIC can also reach remarkably high Q factor value. Due to the distinct Fano line-type, the typical Fano formula [40,41] is employed to fit the modes I and II:

$$T_{Fano}(\omega) = \left| a_1 + ja_2 + \frac{b}{\omega - \omega_0 + j\gamma} \right|^2 \tag{1}$$

where ω_0 is the resonant frequency, a_1, a_2, and b are the constant real numbers, and γ is the overall damping rate of the resonator and distinguishes the line width of the resonance spectra. Utilizing Eq. (1), we can fit the mode I and II of different δ to obtain their Q value. Figure 2(b) and 2(c) present the fitting curves (the black dash lines) of mode I and II when $\delta = 0.12$, which

Optics EXPRESS

are highly consistent with the simulation results (the green and red solid lines in Fig. 2(b) and 2(c), respectively). Then, the Q factor value of mode I and II with different δ can be calculated by $Q = \omega_0/2\gamma$. The deep relationship between the radiative Q-factors and the asymmetric parameters can be revealed by the following expression:

$$Q \propto (\alpha)^{-2} \tag{2}$$

The obtained Q factor value of mode I and II at different δ are shown in Fig. 2(d) and 2(e), respectively, where the Q value of mode I and II both satisfy a linear relationship with α^{-2}. The results further demonstrate that mode I and II are both from symmetry-protected BIC [5,26,42]. The Q factor values of modes I and II can attain nearly infinity when δ is close enough to 0, as shown in Fig. 2(d) and 2(e). As a consequence, the Q-factor value of modes I and II can be engineered by manipulating the asymmetric parameters of the meta-surface.

Subsequently, we employed different semiconductor materials to construct permittivity asymmetry and excite polarization-insensitive dual-band quasi-BICs based on the analysis above. The FG is made of amorphous Si, and then InAs, GaAs, and InP are chosen as candidates of SG. The data used for all materials in this letter refers to the Palik handbook [39], which can boost the reliability of the simulation results. According to the Palik handbook, the refractive indices of the considered materials change with their wavelengths. To better understand the demonstration in Fig. 2(a), however, the average refractive indices of the considered materials in the corresponding wavelength range can be provided as Si for 3.53, InAs for 3.57, GaAs for 3.44, and InP for 3.24. Therefore, the refractive index differences δ of Si-InAs, Si-GaAs, and Si-InP are 0.04, −0.09, −0.29, respectively. Figure 3(a) to 3(c) provide the transmission spectra of Si-InAs, Si-GaAs, and Si-InP, respectively, where they all displayed two Fano-like line-type demonstrated as quasi-BICs. An excellent meta-surface resonator applied to optics and photonics should perform ultra-high Q factor. And its transmission spectrum should be spectrally clean in the desired wavelength range, i.e., without superfluous and clutter modes which can affect the required resonant states. Additionally, a high spectral contrasts ratio and sharp spectral line shape of the required resonant modes are also desired. The spectral contrasts ratio can be defined as

$$[(T_{on} - T_{off})]/[(T_{on} + T_{off})] \times 100\% \tag{3}$$

Herein, T_{on} and T_{off} represent the maximum and minimum transmittance, respectively. Table 1 lists the performance of different material combinations, where $\partial\lambda$ represents the wavelength interval between the resonant peak and anti-peak. One can be observed that they perform comparable spectral contrasts ratios and modulation depths. However, the performances of Q values and $\partial\lambda$ are far better in terms of the combinations of Si-InAs. Additionally, the Q values of the two resonances are basically coincident with the results in Fig. 2. Consequently, the partnership of Si and InAs is employed to the permittivity-asymmetric metasurface. Herein, the dispersion curves of glass, Si, and InAs are displayed in Fig. 3(d)–3(f), respectively, which are obtained based on the experimental data of the Palik handbook. The proposed metasurface can be fabricated by low-pressure chemical vapor deposition (LPCVD) [43] and standard electron-beam lithography (EBL) [44]. We can first deposit amorphous Si by LPCVD, and then etch the required patterns with masks by EBL. Next, the same process can be employed to obtain the required InAs blocks. Finally, we can remove the masks on the Si and InAs blocks to obtain the proposed metasurface. Herein, we named the quasi-BIC modes in Fig. 3(a) as III and IV, respectively, for description conveniently.

3.2. Multipolar resonant analysis in the proposed meta-surface

Differing from traditional electric and magnetic multipoles, toroidal multipoles perform distinct characteristics and have attracted abundant attention in recent years. As one of the most exotic

Optics EXPRESS

Table 1. Performance of different material combinations in the proposed meta-surface

Types	Mode	Q value	spectral contrasts ratio	modulation depth[a]	$\partial\lambda$
Si-InAs	III	4447	92.17%	95.92%	0.4
	IV	11391	98.33 %	99.16%	0.2
Si-GaAs	III	1143	98.99%	99.49%	1.2
	IV	1920	96.41%	98.17%	0.9
Si-InP	III	90	99.99%	99.99%	14
	IV	188	99.98%	99.99%	6.1

[a]**Modulation depth is identified as** $|(\boldsymbol{T}_{\mathbf{on}} - \boldsymbol{T}_{\mathbf{off}})/\boldsymbol{T}_{\mathbf{on}}| \times 100\%$.

multipole families, they have been employed to construe exotic phenomena in non-radiating sources and Aharonov-Bohm effect [45], the anapole modes [28,46,47], optical force on toroidal nanostructures [48], and toroidal meta-surfaces and metamaterials [12,23,26,29,31,49–52]. TD is a basic member of the family, which can enhance the light-matter interactions and is related to the high Q factor, further underlining the importance of being investigated. Nevertheless, they are quite difficult to distinguish because of the similarity of their radiation patterns between a dynamic TD and an electric dipole (ED) resonance. For instance, Mie theory [46,47,53] doesn't display toroidal multipoles explicitly.

Multipolar decomposition in Cartesian is quite suitable to comprehend the underlying physical mechanism and widely used to identify the characteristics of multipolar modes including toroidal multipoles [50], theoretically. We first integrate the carrier density ρ or the displacement current density $\boldsymbol{J}$ in the unit cell with permittivity-asymmetric cuboids tetramer clusters to obtain the different multipole moments. Then, the scattered power of unit cell can be calculated for different multipole moments. Five most important moments are discussed, which are defined as ED: $\boldsymbol{P} = \frac{1}{\mathrm{i}\omega}\int \boldsymbol{j}\mathrm{d}^3r$, magnetic dipole (MD): $\boldsymbol{M} = \frac{1}{2c}\int(\boldsymbol{r}\times\boldsymbol{j})\mathrm{d}^3r$, TD: $\boldsymbol{T} = \frac{1}{10c}\int[(\boldsymbol{r}\cdot\boldsymbol{j})\boldsymbol{r} - 2\boldsymbol{r}^2\boldsymbol{j}]\mathrm{d}^3r$, electric quadrupole (EQ): $\boldsymbol{Q}^{(e)}_{\alpha\beta} = \frac{1}{2i\omega}\int\left[r_\alpha j_\beta + r_\beta j_\alpha - \frac{2}{3}(\boldsymbol{r}\cdot\boldsymbol{j})\delta_{\alpha,\beta}\right]d^3r$, and MQ: $\boldsymbol{Q}^{(m)}_{\alpha\beta} = \frac{1}{3c}\int[(\boldsymbol{r}\times\boldsymbol{j})_\alpha r_\beta + (\boldsymbol{r}\times\boldsymbol{j})_\beta r_\alpha]d^3r$, where ω speaks for the angular frequency, $\boldsymbol{r}$ and c means the displacement vectors and light speed, respectively. Ulteriorly, the scattered powers of the five most important multipoles are calculated in a Cartesian coordinate system and displayed in Fig. 4(a) and (b). For mode III and IV, one can recognize clearly that MQ contributes most among the five multipoles, however, the contribution of TD response can't be ignored. Detailly, mode III is derived from MQ, EQ, and TD. In terms of mode IV, it's activated by MQ and TD. To further identify the contributions of TD response, we calculate the components of TD along different directions. Results in Fig. 4(c) show that the contribution of TD is dominated by the component along the y-axis (Ty) for modes III and IV. Figure 4(d) displays the phase of Ty, where a phase difference π exits between mode III and mode IV. The results in Fig. 4(d) mean the direction of TD is inverse in terms of mode III and mode IV.

To intuitively comprehend the dual quasi-BIC resonances, we visualized the near-field electromagnetic distributions of the permittivity-asymmetric meta-surface at their resonant wavelengths in Fig. 5(a)-(d). Figure 5(a)–5(b) shows the y-component of H-field intensity for mode III and mode IV, respectively. Here, we use black arrows to describe the magnetic field directions. Accordingly, one can be observed that the magnetic fields of cuboids for mode III have opposite directions oriented along the y-axis in the x-y plane, which identifies the typical MQ response. Similarly, the results in Fig. 5(b) prove the presence of MQ for mode IV but show inverse magnetic field directions when compared to the results of mode III. The electric field intensity and direction (red arrows) of mode III and mode IV are provided in Fig. 5(c)-(d), where the electric fields are firmly constrained within the slits of the cuboid tetramer clusters and indicate two peculiar reversed swirls in the x-y plane. They are typically TD responses [25,29,30].

Optics EXPRESS

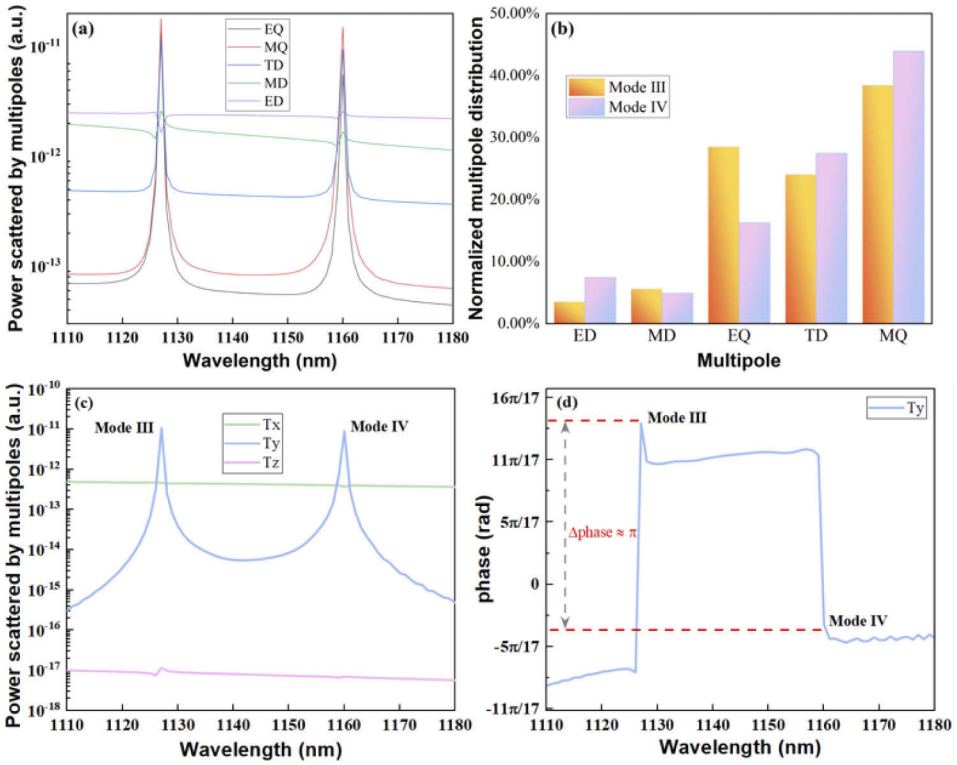

Fig. 4. (a) Radiation powers from different multipoles for mode III and mode IV. (b) The normalized multiple distributions from different multipoles for mode III and mode IV. (c) x, y and z components of TD. (d) The Ty phase of mode III and IV.

The green arrows represent the directions of the TD moment for mode III and mode IV, which are consistent with the analysis of multipolar decomposition results in Fig. 4.

3.3. *Analysis of polarization-insensitive and scalable characteristics*

Due to the structural asymmetry to excite quasi-BICs, most works [12,23,25–28] are polarization-sensitive and can only offer the excitations of quasi-BICs by an incident polarization along the asymmetric direction. However, owing to the symmetric structural parameters, our design manifests the same resonant responses with arbitrary incident polarization, which can support robust responses in our structure with different incident configurations. Figure 6 exhibits the transmission spectra under different polarization angles of the proposed structure to demonstrate the polarization-insensitive characteristic. We define the polarization angle θ as the direction between the $+x$-axis and incident polarization. From Fig. 6(a) and 6(b), one can observe that the transmission spectra of the proposed meta-surface keep unchanged when plane waves with different polarization angles are incident, which can verify the polarization-insensitive characteristic. In addition, the tunable characteristic is also worthwhile to be investigated so that the design can be employed to different wavelength ranges to cater for relevant demands. Therefore, we changed the scalable factor S of the proposed meta-surface and the results are provided in Fig. 6(c). As the scalable factor S increases gradually, the two resonant modes show distinct redshifts, which means that the resonance wavelengths of mode III and IV can be tunable by adjusting the scalable factor S.

Optics EXPRESS

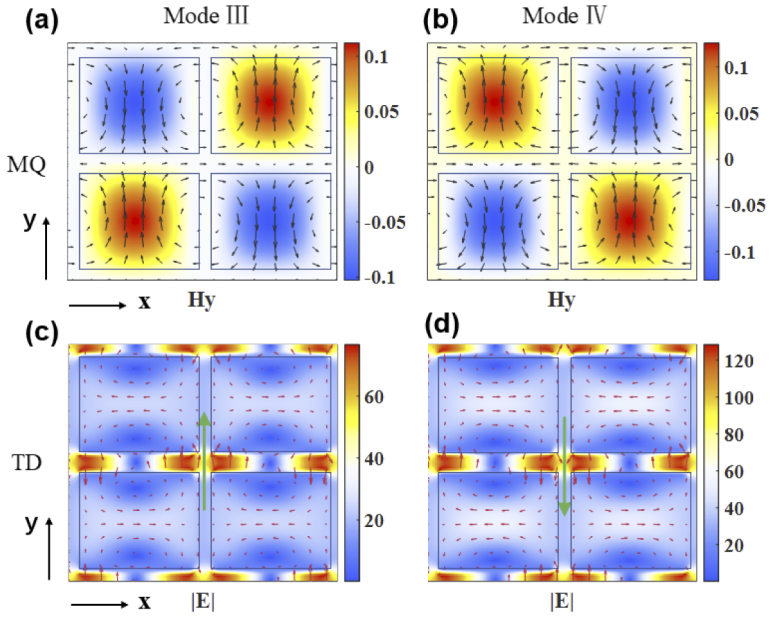

Fig. 5. (a)-(d) Electromagnetic field distribution of mode III (λ = 1127.9 *nm*) and mode IV (λ = 1161.8 *nm*).

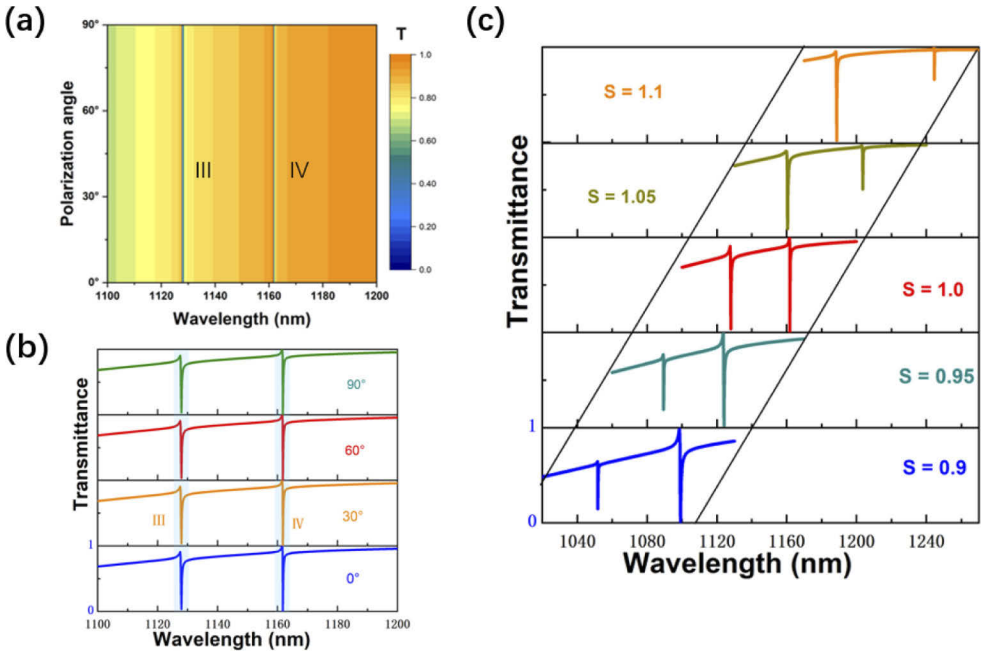

Fig. 6. (a)(b) Transmission spectra with different polarization angles. (c) Transmission spectra under different scalable factor *S*.

3.4. Sensing performance

The dual TD quasi-BIC modes excited by the permittivity-asymmetric meta-surfaces, manifest ultra-high *Q* values so that the meta-surface provides an opportunity to serve as a refractive index

Optics EXPRESS

sensor. Generally, the parameters, sensitivity (S_0) and figure of merit (*FOM*), are employed as key parameters to evaluate the sensing performance of the proposed permittivity-asymmetric meta-surface. We defined the S_0 as the wavelength shift with Unit refractive index change ($S_0 = \Delta\lambda/\Delta n$) and the *FOM* as the ratio of sensitivity to the wavelength interval between the resonant peak and anti-peak ($\delta\lambda$), i.e., $FOM = S_0/\delta\lambda$. Simulation results of the transmission with changing surrounding background medium from 1.0 to 1.1 are offered in Fig. 7(a), where one can observe a distinct redshift for the resonant wavelengths of mode III and mode IV. The accumulative wavelength shifts with increasing refractive index are displayed in Fig. 7(b). One can calculate the sensitivity (the slope of the fitting curves) of the modes. Consequently, the calculated values of S_0 for mode III and mode IV are 170 nm/RIU and 182 nm/RIU, respectively. Accordingly, one can obtain the *FOM* values, which can reach 567 and 910.

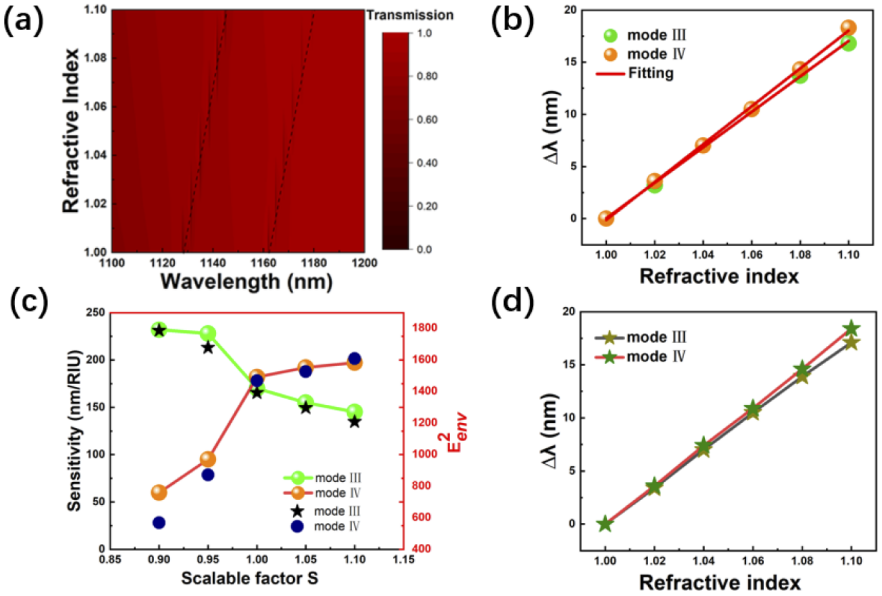

Fig. 7. (a) Transmission spectra with different surrounding gas environments. (b) Resonance wavelength shifts of mode III and IV with different surrounding gas environments based on the simulation results. (c) Sensitivities and average electric field intensity of mode III and IV with different scalable factor *S*. (d) The calculated wavelength shift with different environment permittivity based on perturbation theory.

To further figure out the suitability of the dual TD quasi-BIC resonances for sensing, we investigated the influence of scalable factor S for the permittivity-asymmetric meta-surface (Fig. 7(c)). As shown in Fig. 7(c), mode III and mode IV appear inverse results. The values of sensitivity for mode III drop ceaselessly but for mode IV, the results are increased with the different *S* from 0.9 to 1.1. To distinguish the underlying physical mechanism of this phenomenon, we employed perturbation theory [54]

$$\frac{\delta\omega}{\omega_0} \approx \frac{\int V_{\text{env}}[\varepsilon_{\text{env}}(\mathbf{r}) - \varepsilon_0(\mathbf{r})]|\mathbf{E}(\mathbf{r},\omega_0)|^2 \,\mathrm{d}V}{\int V_{\text{all}}\varepsilon_0(\mathbf{r})|\mathbf{E}(\mathbf{r},\omega_0)|^2 \,\mathrm{d}V} \tag{4}$$

Herein, ω_0 and $\delta\omega$ mean the original resonance frequency and resonance shift, respectively. ε_0 represents the permittivity of the original surrounding medium and ε_{env} serves as the permittivity distribution from the modified local environment. $\mathbf{E}(\mathbf{r}\ ,\ \omega_0)$ is the distributed electric field of the resonant modes in the metasurface. We define the volume V_{all} as a cube of $P \times P \times 350$ nm, where

Optics EXPRESS

the height of 350 nm covers the resonator height (200 nm) and the height above the metasurface top surface. Using V_{all} minus the resonator volume, one can obtain the environment volume (V_{env}). According to Eq. (4), we can conclude that the stronger the electric field confinement of the resonant mode outside the resonator in the V_{env}, the larger the value of $\delta\omega$, i.e., the higher the sensitivity. Hence, we calculated the values of E^2_{env} for the proposed metasurfaces with changing S at their resonant wavelengths, where E^2_{env} is the average intensity of the electric field in the V_{env}. The results are displayed in Fig. 7(c) (black stars and navy spheres represent mode III and mode IV, respectively). When S increases from 0.9 to 1.1, the near-field enhances for mode III keep cutting down, but the results for mode IV are totally inverse. The results are consistent with the analysis above. That can explain the inverse behavior in terms of the sensitivity with the different S from 0.9 to 1.1. Additionally, the theoretical wavelength shift with different environment permittivity can be calculated based on Eq. (4). Figure 4(d) illustrates the calculated results of mode III and mode IV, where we calculated the sensitivity as 171 nm/RIU and 184 nm/RIU. The results are nearly the same as the simulation values in Fig. 4(b).

4. Conclusion

In this paper, we propose and theoretically demonstrate a permittivity-asymmetric all-dielectric meta-surface, which can support dual-band polarization-insensitive TD quasi-BIC modes. Selecting the combination of Si and InAs as the permittivity-asymmetric materials, the dual resonant modes yield ultra-high Q values of 4447 and 11391, respectively. By multipolar decomposition in cartesian and electromagnetic distributions, we conclude that the dual-band quasi-BIC modes are both governed by MQ and TD. Additionally, we demonstrate the polarization-insensitive and scalable characteristics of the permittivity-asymmetric meta-surface. Sensing performances are also evaluated. Sensitivities and *FOM* values of the dual resonant modes are 170 nm/RIU, 567 and 182 nm/RIU, 910, respectively. As an instance, our work offers an uncommon route to design dual-band polarization-insensitive TD quasi-BICs resonators and facilitates their applications in optic and photonics, such as low-threshold lasers and sensing.

Funding. National Natural Science Foundation of China (61372035, 61531007, 61835002); China Scholarship Council (CSC No. 202006470074); BUPT Excellent Ph.D. Students Foundation (CX2021307).

Acknowledgments. We thank the support of the National Natural Science Foundation of China (61372035, 61531007, 61835002); Beijing University of Posts and Telecommunications (CX2021307); the China Scholarship Council (CSC No. 202006470074).

Disclosures. The authors declare no conflicts of interest.

Data availability. Data underlying the results presented in this paper are not publicly available at this time but may be obtained from the authors upon reasonable request.

References

1. A. M. Tamim, M. M. Hasan, M. R. I. Faruque, M. T. Islam, and J. Nebhen, "Polarization-independent symmetrical digital metasurface absorber," Results Phys. **24**, 103985 (2021).
2. Y. Kang, J. Zhang, H. Liu, Y. He, and J. Zhang, "Tunable dual-band metamaterial absorber at deep-subwavelength scale," Results Phys. **27**, 104525 (2021).
3. J. Gu, R. Singh, X. Liu, X. Zhang, Y. Ma, S. Zhang, S. A. Maier, Z. Tian, A. K. Azad, H. Chen, A. J. Taylor, J. Han, and W. Zhang, "Active control of electromagnetically induced transparency analogue in terahertz metamaterials," Nat Commun **3**(1), 1151 (2012).
4. R. Singh, W. Cao, I. Al-Naib, L. Cong, W. Withayachumnankul, and W. Zhang, "Ultrasensitive terahertz sensing with high-Q Fano resonances in metasurfaces," Appl. Phys. Lett. **105**(17), 171101 (2014).
5. L. Yang, S. Yu, H. Li, and T. Zhao, "Multiple Fano resonances excitation on all-dielectric nanohole arrays metasurfaces," Opt. Express **29**(10), 14905–14916 (2021).
6. M. Tonouchi, "Cutting-edge terahertz technology," Nat. Photonics **1**(2), 97–105 (2007).
7. N. Meinzer, W. L. Barnes, and I. R. Hooper, "Plasmonic meta-atoms and metasurfaces," Nat. Photonics **8**(12), 889–898 (2014).
8. N. Dabidian, I. Kholmanov, A. B. Khanikaev, K. Tatar, S. Trendafilov, S. H. Mousavi, C. Magnuson, R. S. Ruoff, and G. Shvets, "Strong Modulation of Infrared Light using Graphene Integration with Plasmonic Fano-Resonant Metasurfaces," ACS Photonics **2**(2), 216–227 (2015).

Optics EXPRESS

9. P. Mandal, "H-Shape Plasmonic Metasurface as Refractive Index Sensor," Plasmonics **10**(2), 439–445 (2015).
10. M. Allione, V. V. Temnov, Y. Fedutik, U. Woggon, and M. V. Artemyev, "Surface plasmon mediated interference phenomena in low-Q silver nanowire cavities," Nano Lett. **8**(1), 31–35 (2008).
11. A. I. Kuznetsov, A. E. Miroshnichenko, M. L. Brongersma, Y. S. Kivshar, and B. Luk'yanchuk, "Optically resonant dielectric nanostructures," Science **354**(6314), 2472 (2016).
12. X. Liu, J. Li, Q. Zhang, and Y. Wang, "Dual-toroidal dipole excitation on permittivity-asymmetric dielectric metasurfaces," Opt. Lett. **45**(10), 2826–2829 (2020).
13. H. Liu, L. Zheng, P. Ma, Y. Zhong, B. Liu, X. Chen, and H. Liu, "Metasurface generated polarization insensitive Fano resonance for high-performance refractive index sensing," Opt. Express **27**(9), 13252–13262 (2019).
14. A. Forouzmand and H. Mosallaei, "All-dielectric c-shaped nanoantennas for light manipulation: Tailoring both magnetic and electric resonances to the desire," Adv. Opt. Mater. **5**(14), 1700147 (2017).
15. J. von Neumann and E. P. Wigner, "Über merkwürdige diskrete eigenwerte," Phys. Zschr. **30**, 294–297 (1929).
16. L. Ni, Z. Wang, C. Peng, and Z. Li, "Tunable optical bound states in the continuum beyond in-plane symmetry protection," Phys. Rev. B **94**(24), 245148 (2016).
17. C. W. Hsu, B. Zhen, A. D. Stone, J. D. Joannopoulos, and M. Soljačić, "Bound states in the continuum," Nat. Rev. Mater. **1**(9), 16048 (2016).
18. P. Yu, A. S. Kupriianov, V. Dmitriev, and V. R. Tuz, "All- dielectric metasurfaces with trapped modes: Group-theoretical description," J. Appl. Phys. **125**(14), 143101 (2019).
19. H. Friedrich and D. Wintgen, "Interfering resonances and bound states in the continuum," Phys. Rev. A **32**(6), 3231–3242 (1985).
20. M. V. Rybin, K. L. Koshelev, Z. F. Sadrieva, K. B. Samusev, A. A. Bogdanov, M. F. Limonov, and Y. S. Kivshar, "High-Q Supercavity Modes in Subwavelength Dielectric Resonators," Phys. Rev. Lett. **119**(24), 243901 (2017).
21. S. Romano, G. Zito, S. N. L. Yépez, S. Cabrini, E. Penzo, G. Coppola, I. Rendina, and V. Mocellaark, "Tuning the exponential sensitivity of a bound-state-in-continuum optical sensor," Opt. Express **27**(13), 18776 (2019).
22. K. Koshelev, S. Lepeshov, M. Liu, A. Bogdanov, and Y. Kivshar, "Asymmetric Metasurfaces with High-Q Resonances Governed by Bound States in the Continuum," Phys. Rev. Lett. **121**(19), 193903 (2018).
23. J. F. Algorri, F. Dell'Olio, P. Roldán-Varona, L. Rodríguez-Cobo, J. M. López-Higuera, J. M. Sánchez-Pena, and D. C. Zografopoulos, "Strongly resonant silicon slot metasurfaces with symmetry-protected bound states in the continuum," Opt. Express **29**(7), 10374–10385 (2021).
24. Z. F. Sadrieva, I. S. Sinev, K. L. Koshelev, A. Samusev, I. V. Iorsh, O. Takayama, R. Malureanu, A. A. Bogdanov, and A. V. Lavrinenko, "Transition from optical bound states in the continuum to leaky resonances: Role of substrate and roughness," ACS Photonics **4**(4), 723–727 (2017).
25. B. Li, J. Yao, H. Zhu, G. Cai, and Q. Liu, "Asymmetric excitations of toroidal dipole resonance and the magnetic dipole quasi-bound state in the continuum in an all-dielectric metasurface," Opt. Mater. Express **11**(7), 2359–2368 (2021).
26. S. Yu, H. Li, Y. Wang, Z. Gao, T. Zhao, and J. Yu, "Multiple Fano resonance excitation of all-dielectric nanoholes cuboid arrays in near infrared region," Results Phys. **28**, 104569 (2021).
27. H. Li, S. Yu, L. Yang, and T. Zhao, "High Q-factor multi-Fano resonances in all-dielectric double square hollow metamaterials," Opt. Laser Technol. **140**, 107072 (2021).
28. W. Wang, X. Zhao, L. Xiong, L. Zheng, Y. Shi, Y. Liu, and J. Qi, "Broken symmetry theta-shaped dielectric arrays for a high Q-factor Fano resonance with anapole excitation and magnetic field tunability," OSA Continuum **2**(2), 507–514 (2019).
29. X. Luo, X. Li, T. Lang, X. Jing, and Z. Hong, "Excitation of high Q toroidal dipole resonance in an all-dielectric metasurface," Opt. Mater. Express **10**(2), 358–368 (2020).
30. Y. Cai, Y. Huang, K. Zhu, and H. Wu, "Symmetric metasurface with dual band polarization-independent high-Q resonances governed by symmetry-protected BIC," Opt. Lett. **46**(16), 4049–4052 (2021).
31. X. Wang, S. Li, and C. Zhou, "Polarization-independent toroidal dipole resonances driven by symmetry-protected BIC in ultraviolet region," Opt. Express **28**(8), 11983–11989 (2020).
32. A. Sayanskiy, A. S. Kupriianov, S. Xu, P. Kapitanova, V. Dmitriev, V. V. Khardikov, and V. R. Tuz, "Controlling high-Q trapped modes in polarization-insensitive all-dielectric metasurfaces," Phys. Rev. B **99**(8), 085306 (2019).
33. A. C. Overvig, S. C. Malek, M. J. Carter, S. Shrestha, and N. Yu, "Selection rules for quasi-bound states in the continuum," Phys. Rev. B **102**(3), 035434 (2020).
34. H. Ahmed, A. Rahim, H. Maab, M. M. Ali, and S. Naureen, "Polarization insensitive all-dielectric metasurfaces for the ultraviolet domain," Opt. Mater. Express **10**(4), 1083–1091 (2020).
35. V. Dmitriev, S. Kupriianov A, S. Santos, and V. R. Tuz, "Symmetry analysis of trimer-based all-dielectric metasurfaces with toroidal dipole modes," J. Phys. D: Appl. Phys. **54**(11), 115107 (2021).
36. Y. He, G. Guo, T. Feng, Y. Xu, and A. E. Miroshnichenko, "Toroidal dipole bound states in the continuum," Phys. Rev. B **98**(16), 161112 (2018).
37. D. C. Zografopoulos and V. Dmitriev, "Quasi-Dark Resonances in Silicon Metasurface for Refractometric Sensing and Tunable Notch Filtering," J. Lightwave Technol. **39**(21), 6985–6993 (2021).
38. J. F. Algorri, D. C. Zografopoulos, A. Ferraro, B. García-Cámara, R. Beccherelli, and J. M. Sánchez-Pena, "Ultrahigh-quality factor resonant dielectric metasurfaces based on hollow nanocuboids," Opt. Express **27**(5), 6320–6330 (2019).

Optics EXPRESS

39. E. D. Palik, "Handbook of Optical Constants of Solids," Academic **2**, 1 (1985)..
40. Z. Sadrieva, K. Frizyuk, M. Petrov, Y. Kivshar, and A. Bogdanov, "Multipolar origin of bound states in the continuum," Phys. Rev. B **100**(11), 115303 (2019).
41. L. Xu, K. Z. Kamali, L. J. Huang, M. Rahmani, A. Smirnov, R. Camacho-Morales, Y. X. Ma, G. Q. Zhang, M. Woolley, D. Neshev, and A. E. Miroshnichenko, "Dynamic Nonlinear Image Tuning through Magnetic Dipole Quasi-BIC Ultrathin Resonators," Adv. Sci. **6**(15), 1802119 (2019).
42. K. Koshelev, A. Bogdanov, and Y. Kivshar, "Meta-optics and bound states in the continuum," Sci. Bull. **64**(12), 836–842 (2019).
43. Y. F. Yu, A. Y. Zhu, R. Paniagua-Domínguez, Y. H. Fu, B. Luk'yanchuk, and A. I. Kuznetsov, "High-transmission dielectric metasurface with 2π phase control at visible wavelengths," Laser Photonics Rev. **9**(4), 412–418 (2015).
44. P. A. Jeong, M. D. Goldflam, S. Campione, J. L. Briscoe, P. P. Vabishchevich, J. Nogan, M. B. Sinclair, T. S. Luk, and I. Brener, "High quality factor toroidal resonances in dielectric metasurfaces," ACS Photonics **7**(7), 1699–1707 (2020).
45. N. A. Nemkov, A. A. Basharin, and V. A. Fedotov, "Nonradiating sources, dynamic anapole, and Aharonov-Bohm effect," Phys. Rev. B **95**(16), 165134 (2017).
46. V. A. Fedotov, A. V. Rogacheva, V. Savinov, D. P. Tsai, and N. I. Zheludev, "Resonant Transparency and Non-Trivial Non-Radiating Excitations in Toroidal Metamaterials "," Sci. Rep. **3**(1), 2967 (2013).
47. A. E. Miroshnichenko, A. B. Evlyukhin, Y. F. Yu, R. M. Bakker, A. Chipouline, A. I. Kuznetsov, B. Luk'yanchuk, B. N. Chichkov, and Y. S. Kivshar, "Nonradiating anapole modes in dielectric nanoparticles," Nat. Commun. **6**(1), 8069 (2015).
48. X. L. Zhang, S. B. Wang, Z. F. Lin, H. B. Sun, and C. T. Chan, "Optical force on toroidal nanostructures: Toroidal dipole versus renormalized electric dipole," Phys. Rev. A **92**(4), 043804 (2015).
49. K. Marinov, A. D. Boardman, V. A. Fedotov, and N. Zheludev, "Toroidal metamaterial," New J. Phys. **9**(9), 324 (2007).
50. T. Kaelberer, V. A. Fedotov, N. Papasimakis, D. P. Tsai, and N. I. Zheludev, "Toroidal Dipolar Response in a Metamaterial," Science **330**(6010), 1510–1512 (2010).
51. Z. G. Dong, P. Ni, J. Zhu, X. B. Yin, and X. Zhang, "Toroidal dipole response in a multifold double-ring metamaterial," Opt. Express **20**(12), 13065 (2012).
52. Y. W. Huang, W. T. Chen, P. C. Wu, V. Fedotov, V. Savinov, Y. Z. Ho, Y. F. Chau, N. I. Zheludev, and D. P. Tsai, "Design of plasmonic toroidal metamaterials at optical frequencies," Opt. Express **20**(2), 1760 (2012).
53. N. Papasimakis, V. A. Fedotov, V. Savinov, T. A. Raybould, and N. I. Zheludev, "Electromagnetic toroidal excitations in matter and free space," Nat. Mater. **15**(3), 263–271 (2016).
54. I. Teraoka and S. Arnold, "Theory of resonance shifts in TE and TM whispering gallery modes by nonradial perturbations for sensing applications," J. Opt. Soc. Am. B **23**(7), 1381–1389 (2006).